ORIGINAL SCIENTIFIC PAPER

CROATICA CHEMICA ACTA

*Croat. Chem. Acta* **2017**, *90*(*4*), 613–623
Published online: April 11, 2018
DOI: 10.5562/cca3270

HKD 1926

# A Case Study of Supramolecular Organization: One Ferrocene Substituted Iminodiacetamide and its Chloroform Solvate

Natalija P. Juraj, Jeremy Le Pennec, Berislav Perić, Srećko I. Kirin*

Ruđer Bošković Institute, Bijenička c. 54, HR-10000 Zagreb, Croatia

* Corresponding author's e-mail address: Srecko.Kirin@irb.hr

RECEIVED: December 18, 2017 ✶ REVISED: February 13, 2018 ✶ ACCEPTED: March 26, 2018

THIS PAPER IS DEDICATED TO PROF. MLADEN ŽINIĆ ON THE OCCASION OF HIS 70TH BIRTHDAY

**Abstract:** This paper describes the synthesis of an amide based conjugate of ferrocene (**Fc**), ethylenediamine (**eda**) and iminodiacetamide (**imda**), **Fc-eda-imda** (**2**). The compound (**2**) is characterized by various spectroscopic, crystallographic and thermoanalytical techniques in solid state and in solution. By crystallization of the title compound **2** from methanol or chloroform, two different crystalline forms **2a** and **2b** were obtained, respectively. In their X-ray single crystal structures, **2a** and **2b** reveal similar 2D hydrogen bonding networks, but differ by supramolecular organization, namely aromatic π – π stacking interactions in the third spatial dimension.

**Keywords**: amides, ferrocene, hydrogen bonding, iminodiacetamide, supramolecular chemistry.

## INTRODUCTION

THE field of supramolecular chemistry, defined as "chemistry beyond the molecule", has progressed greatly since Charles Pedersen's discovery of crown ethers that exhibit host-guest interactions.[1] Supramolecular chemistry, based on molecules held together by noncovalent interactions such as hydrogen bonds, electrostatic, van der Waals, π---π stacking or hydrophobic interactions, is a wide field of study, with many applications,[2] such as sensing,[3] molecular machines,[4] drug delivery[5] and catalysis.[6]

In supramolecular chemistry, the secondary amide group is an important building block that is a starting point for understanding the formation of secondary and tertiary protein structures. When adopting such structures, proteins rely on noncovalent interactions, such as H-bonds between the amide groups that can act both as H-bond donors (N-H) and H-bond acceptors (C=O).[7] Amide derived iminodiacetamide (**imda**) derivatives are well known ligands for late transition metals that give access to a great variety of structural motifs.[8,9] In addition, the stability of amide conjugated ferrocenoly group in aerobic media, and aqueous as well as organic solvents, gives access to a large variety of derivatives, and its favorable electrochemical properties have made ferrocene and its derivatives very popular molecules for biological applications and for conjugation with biomolecules.[10]

In this work, we present the crystal and molecular structures of two crystalline forms of a ferrocene amide conjugate **Fc-eda-imda**, **2a**, and **Fc-eda-imda × CDCl$_3$**, **2b**. The difference between the bulk solid state structures of **2$_{MeOH}$** and **2$_{CHCl3}$** is described in detail, using single crystal and powder X-ray diffraction, differential scanning calorimetry and thermogravimetry. Also, the difference between the structure in the solid state and in $CHCl_3$ solution is studied with $^1$H NMR and IR spectroscopy.

## EXPERIMENTAL

**General remarks.** Reactions were carried out in ordinary glassware and chemicals were used as purchased from commercial suppliers without further purification. The synthesis of **2** was carried out in a microwave reactor (CEM

Discover). Reactions were monitored by TLC on silica gel 60 $F_{254}$ plates and detected with a UV lamp (254 nm); crude products were purified using automated flash chromatography (Teledyne Isco CombiFlash Rf) equipped with a UV detector (254 nm) and pre-packed silica columns.

Mass spectra were recorded on a HPLC-MS system (Agilent Technologies 1200) coupled with a 6410 Triple-Quadrupole mass spectrometer, operating in a positive ESI mode. NMR spectra were obtained on a Bruker Avance 300 or 600 spectrometer, operating at 300 or 600 MHz for $^1$H and 75 or 150 MHz for $^{13}$C, the spectra were recorded at room temperature. Chemical shifts, $\delta$ (ppm), indicate a downfield shift from the internal standard, tetramethylsilane, TMS. Coupling constants, *J*, are given in Hz. Infrared spectra were recorded using KBr pellets or in chloroform solution (in a KBr solution cell) with a Bruker Alpha FT-IR spectrometer, in the 4000–350 cm$^{-1}$ region. The UV-Vis spectra were recorded on Varian Cary 50 spectrophotometer using a 1 cm Suprasil quartz cell.

For the DSC measurements approximately 2–5 mg of sample was placed in a standard aluminum crucible (40 µL) and heated at a 10°C/min rate in the temperature range 25–500 °C, under nitrogen flow of 180 mL/min using a Mettler-Toledo DSC 823$^e$ instrument. For the thermogravimetry measurements approximately 5–7 mg of sample was placed in a standard platinum crucible (140 µL), heated at a 10 °C/min rate, under flow of 50 mL/min air, in the temperature range of 25−1000 °C on a Shimadzu DTG-60H instrument.

The powder diffractograms were measured on a PANalytical Aeris instrument; conditions: Bragg-Brentano geometry ($\theta$–$2\theta$), source Cu-Kα ($\lambda$ = 1.5418 Å), measurement from 5° to 70° ($2\theta$), with 5.2°/min (0.0216° step and 0.25 s/step). Consistency of sample $\mathbf{2_{MeOH}}$ with single crystal structure **2a** have been checked by LaBail fit of powder data in the $2\Theta$ region of 5°–32°, while for sample $\mathbf{2_{CHCl3}}$ the phase analysis was performed using both structural models from the single crystal data (**2a** and **2b**), in the $2\Theta$ region of 5°–28°. The calculations were performed by using GSAS and EXPGUI programs.[11,12]

**X-ray single crystal diffraction**. The X-ray intensity data were collected on Oxford diffraction Xcalibur CCD diffractometer using monochromatic Cu-Kα ($\lambda$ = 1.54184 Å) radiation at 293 K. The data were processed with CrysalisPro program[13] (unit cell determination and data reduction). Both crystals were of low quality: **2b** diffracted poorly at high angles and reflections up to $\Theta_{max}$ = 59° were taken into calculations, while for **2a** reflections up to $\Theta_{max}$ = 76° were used. For **2b**, lower number of reflections and lower quality of measured intensities at high angles resulted in a relatively high R value (14.19 %), although procedure of solving the crystal structure by direct methods[14] undoubtedly recognized the correct form of the molecule, plus several peaks in residual density were interpreted as an additional chloroform solvate molecule. During indexation of the measured CCD frames for **2b** (which were collected after compound **2a**), it was clear that unit cell volume of **2b** is slightly larger than one half of the unit cell of **2a**, confirming assumption of an additional smaller molecule in the unit cell (chloroform). For **2a** the unit cell dimensions were consistent with eight **Fc-eda-imda** molecules. Lower number of reflections for **2b** also led to low precision of C–C bonds and large Hirshfeld differences for some atoms in the structure (C28 and C29).[15] During refinement of both structures with SHELXL program,[16] all non-hydrogen atoms were treated anisotropically. For **2b**, displacement parameters for carbon atoms in ferrocene unit were restrained to isotropic values (ISOR restrain). Also, the occupancy of chloroform was refined using additional free variable (FVAR). All hydrogen atoms were included in the model at geometrically calculated positions and refined using riding model. As crystals of **2b** were grown from deuterated chloroform, deuterium has been explicitly included in UNIT and SFAC instructions, as well as in the atom list. Experimental data for X-ray diffraction studies in this publication are collected in Table 1. The structures are deposited in CCDC database and numbers 1811729 and 1811730 contain the supplementary crystallographic data for this paper. These data can be obtained free of charge from The Cambridge Crystallographic Data Centre via www.ccdc.cam.ac.uk/data_request/cif.

**2-Chloro-*N*-phenylacetamide**.[17] A solution of aniline (9.13 mL, 0.10 mol) in acetic acid (conc., 85 mL) was cooled to 10 °C and chloroacetyl chloride (8.75 mL, 0.11 mol) was added at once. With vigorous stirring, a solution of $CH_3COONa \times 3H_2O$ (33 g, 0.24 mol) in 140 mL of water was rapidly added. After 30 minutes, the precipitated product was filtered under vacuum through a Büchner funnel, washed with water and dried. No further purification was required. Yield: 13.9 g (0.08 mol, 82%), white powder, $R_f$ = 0.62, 5% methanol in dichloromethane. $^1$H NMR (300 MHz, $CD_3CN$) $\delta$/ppm: 8.57 (s, 1H), 7.61–7.51 (m, 2H), 7.41–7.29 (m, 2H), 7.14 (t, *J* = 7.4 Hz, 1H), 4.15 (s, 2H).

**Ferrocene-CO-NH-CH$_2$-CH$_2$-NH-Boc**, **Fc-eda-boc** (**1**).[18,19] A solution of ferrocenecarboxylic acid (232.1 mg, 1 mmol), DIPEA (680 µL, 4 mmol), TBTU (321.1 mg, 1 mmol) and HOBt (135.1 mg, 1 mmol) in dichloromethane (20 ml) was stirred at room temperature for 1 hour. *N*-Boc-ethylenediamine (158 µL, 1 mmol) was added and the stirring continued for 2 days. The reaction mixture was washed with $NaHCO_3$, brine and citric acid, the organic layer dried over anhydrous sodium sulfate, filtered and

**Table 1.** Crystal data and details of crystal structure refinement for **2a** and **2b**

| Compound | **2a** | **2b** |
|---|---|---|
| Empirical formula | $C_{29}H_{30}FeN_4O_3$ | $C_{29}H_{30}FeN_4O_3 \cdot 0.95\ CDCl_3$ |
| Formula weight | 538.42 | 652.78 |
| Temperature/K | 293(2) | 293(2) |
| $\lambda$/Å (Cu $K_\alpha$) | 1.54184 | 1.54184 |
| Crystal system | monoclinic | monoclinic |
| Space group | $P2_1/c$ | $P2_1/c$ |
| $a$/Å | 9.3748(2) | 16.9956(11) |
| $b$/Å | 19.4702(4) | 19.5977(8) |
| $c$/Å | 30.0352(7) | 9.3479(4) |
| $\alpha$/Å | 90 | 90 |
| $\beta$/Å | 105.323(2) | 94.123(5) |
| $\gamma$/Å | 90 | 90 |
| $V$/Å$^3$ | 5287.4(2) | 3105.5(3) |
| $Z$ | 8 | 4 |
| $D_{calc}$/mg/mm$^3$ | 1.353 | 1.396 |
| $\mu$/mm$^{-1}$ | 4.877 | 6.456 |
| Crystal size/mm$^3$ | 0.3 × 0.25 × 0.2 | 0.3 × 0.25 × 0.2 |
| $\Theta_{min}$, $\Theta_{max}$ /° | 3.05, 76.03 | 4.51, 58.93 |
| Reflections collected | 35239 | 9352 |
| Independent reflections | 10782 ($R_{int}$ = 0.0914) | 4410 ($R_{int}$ = 0.1083) |
| Data/restraints/parameters | 10782/0/667 | 4410/66/371 |
| $R_1$[(a)] [I > 2σ(I)] | 0.1049 | 0.1419 |
| $wR_2$[(b)](all data) | 0.3142 | 0.3973 |
| GOF[(c)] | 1.011 | 1.059 |
| Largest diff. peak/hole/e Å$^{-3}$ | 0.698/–1.270 | 0.946 / –0.820 |

(a) $R_1 = \sum ||F_o| - |F_c|| / \sum |F_o|$.
(b) $wR_2 = \{\sum[w(F_o^2 - F_c^2)^2] / \sum[w(F_o^2)^2]\}^{1/2}$.
(c) GOF = $\{\sum[w(F_o^2 - F_c^2)^2]/(n-p)\}^{1/2}$, where $n$ is the number of reflections and $p$ is the total number of parameters refined.

evaporated in a vacuum. The crude product was purified by automated flash chromatography (20 % to 80 % ethyl-acetate in *n*-hexane), $R_f$ = 0.13, EtOAc : hexane = 1 : 1. Yield: 276.7 mg (0.74 mmol, 74 %) of orange powder, $M_r$ ($C_{18}H_{24}FeN_2O_3$) = 372.24. ESI-MS (*m/z*): 395.0 (M+Na$^+$, 66%), 767.1 (2M+Na$^+$, 67%). $^1$H NMR (300 MHz, $CDCl_3$) $\delta$/ppm: 6.56 (s, 1H), 5.03 (s, 1H), 4.76–4.62 (m, 2H), 4.41–4.28 (m, 2H), 4.21 (s, 5H), 3.56 – 3.43 (m, 2H), 3.37 (t, $J$ = 5.6 Hz, 2H), 1.46 (s, 9H) $^{13}$C NMR (150 MHz, $CDCl_3$) $\delta$/ppm: 171.20, 157.40, 79.95, 76.09, 70.55, 69.90, 68.30, 41.22, 40.82, 28.57. IR (KBr) $\tilde{\nu}_{max}$/cm$^{-1}$: 3374, 3245, 3002, 2976, 2928, 2880, 1687, 1640, 1536, 1453, 1364, 1267, 1170, 1018, 819, 718, 504, 486. IR ($CHCl_3$, 40 mmol/L) $\tilde{\nu}_{max}$/cm$^{-1}$: 3449, 3364, 3008, 2982, 2930, 1700, 1643, 1517, 1368, 1285, 1250, 1167, 998, 826, 483. UV-Vis ($CHCl_3$) $\lambda_{max}$ ($\varepsilon$): 443 (219), 350 (431), 306 (1000).

**Ferrocene-CO-NH-CH$_2$-CH$_2$-imda, Fc-eda-imda (2)**.
**Boc-deprotection**: **Fc-eda-boc** (178.7 mg, 0.5 mmol) was dissolved in dichloromethane (7 ml), then TFA (7 ml) was added and the solution was stirred for 2 hours. The mixture was evaporated and dissolved again in dichloromethane. DIPEA was added dropwise until the mixture was neutralized. The crude product **Fc-eda-H** was evaporated in a vacuum and used in the next step without purification. **Amide coupling**: A solution of 2-chloro-*N*-phenylacetamide (203.4 mg, 1.2 mmol), **Fc-eda-H** (after Boc-deprotection of **Fc-eda-boc** (**1**), 131.6 mg, 0.5 mmol), KI (79.7 mg, 0.5 mmol), DIPEA (327 µL, 1.92 mmol) in DMF (8 mL) was stirred in a round bottom flask equipped with a condenser in a microwave reactor (50 W, 100 °C) for 1 hour. The reaction was allowed to cool to room temperature. The mixture was dissolved in 80 mL of ethyl-acetate and then washed with $NaHCO_3$ and brine, the organic layer dried over anhydrous sodium sulfate, filtered and evaporated in a vacuum. The crude product was purified by automated flash chromatography (0 % to 10 % methanol in dichloro-methane), $R_f$ = 0.38, 5 % methanol in dichloromethane. Yield: 133.6 mg (0.247 mmol, 51.5 %), orange powder. $M_r$ ($C_{29}H_{30}FeN_4O_3$) = 538.42. ESI-MS (*m/z*): 561.1 (M+Na$^+$, 11%), 539.1 (M+H$^+$, 100%), 256.0 (Fc-eda$^+$, 6 %). $^1$H NMR (300 MHz, $CDCl_3$) $\delta$/ppm: 9.20 (s, 2H), 7.62 (d, J = 7.7 Hz, 4H), 7.36 – 7.23 (m, 4H), 7.09 (t, J = 7.4 Hz, 2H), 6.76 (t, J = 6.0 Hz, 1H), 4.85 – 4.71 (m, 2H), 4.40 – 4.30 (m, 2H), 4.14 (s, 5H), 3.62 – 3.49 (m, 2H), 3.45 (s, 4H), 2.89 – 2.76 (m, 2H). $^{13}$C NMR (75 MHz, $CDCl_3$) δ/ppm: 171.90, 169.06, 137.70, 128.96, 124.42, 119.84, 75.55, 70.79, 69.77, 68.31, 60.21, 57.04, 37.91. IR (KBr) $\tilde{\nu}_{max}$/cm$^{-1}$: 3276, 3132, 3069, 2935, 2883, 1661, 1632, 1599, 1548, 1445, 1307, 1253, 1179, 821, 755, 692, 499, 484. IR ($CHCl_3$, 20 mmol/L) $\tilde{\nu}_{max}$/cm$^{-1}$: 3283, 3008, 2834, 1679, 1639, 1600, 1532, 1445, 1316, 1297, 489, 482. UV-Vis ($CHCl_3$): $\lambda_{max}$ ($\varepsilon$) = 443 (277), 347 (987), 308 (1214).

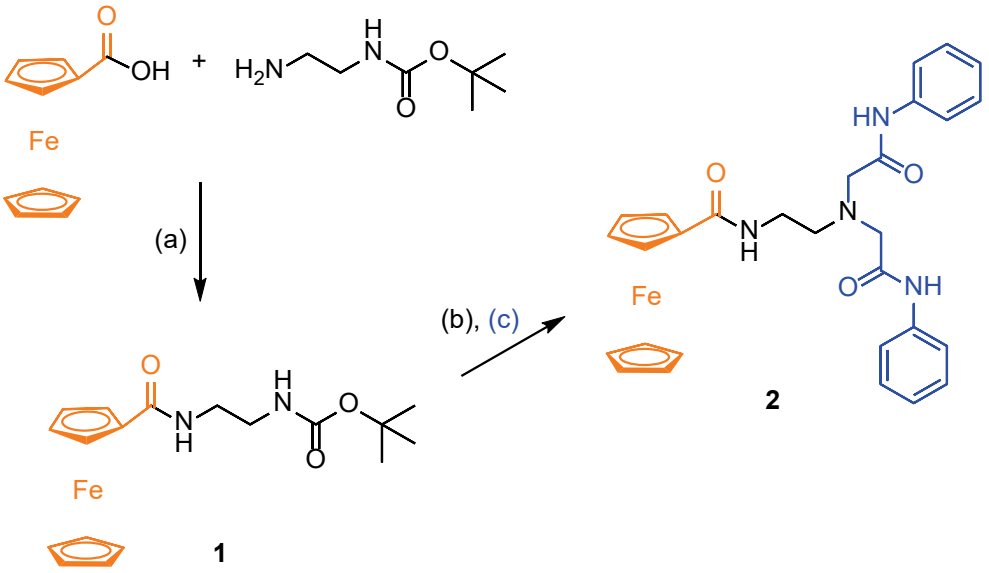


Scheme 1. Reaction conditions. (a) HOBt, TBTU, DIPEA, DCM, 2 days, r.t; (b) DCM, TFA (1:1), 2h; (c) Ph-NH-CO-$CH_2$-Cl, KI, DIPEA, DMF, microwave, 50 W, 100 °C, 1 h.

**Preparation of crystals suitable for X-ray single crystal analysis**. In the first experiment, **Fc-eda-imda** (25 mg) was dissolved in methanol (5 mL) and left in a partly covered vial at room temperature for slow evaporation. After 5 days, flower-like crystals of **2a** were obtained. In a second experiment, **Fc-eda-imda** (1 mg) was dissolved in $CDCl_3$ (0.5 mL) and left in a NMR tube for slow evaporation. After 3 months, needle-like crystals of **2b** were obtained.

**Preparation of samples for powder X-ray diffraction, thermal analysis and IR spectrometry**. **Fc-eda-imda** (41.3 mg and 40.9 mg) was dissolved in methanol (7 mL) or chloroform (10 mL) respectively and left in a partly covered vial at room temperature for slow evaporation. After 2 days, the volume of the solutions was reduced to 2 mL by rotary evaporation and after 5 days, orange flower-like crystals ($\mathbf{2}_{\mathbf{MeOH}}$) were obtained from the methanol solution and a mixture of orange flower-like and needle-like crystals ($\mathbf{2}_{\mathbf{CHCl3}}$) was obtained from the chloroform solution.

## RESULTS AND DISCUSSION

### Synthesis and Basic Characterization

The title compound **Fc-eda-imda** (**2**) was obtained in two synthetic steps in solution, Scheme 1. In the first step, **Fc-eda-boc** (**1**) was synthesized by amide coupling of commercially available precursors, ferrocenecarboxylic acid and *N*-boc-ethylenediamine. The desired **Fc-eda-imda** ligand was prepared in a second synthetic step, where the Boc protecting group of **Fc-eda-boc** was removed in standard conditions (TFA in DCM), and the free primary amine group subsequently reacted in a microwave enhanced nucleophilic substitution reaction with 2-chloro-*N*-phenylacetamide in DMF with the addition of KI.

Crystals suitable for X-ray single crystal analysis were grown from methanol (**2a**) or chloroform (**2b**). The corresponding bulk powder samples, $\mathbf{2}_{\mathbf{MeOH}}$ (obtained from methanol) and $\mathbf{2}_{\mathbf{CHCl3}}$ (obtained from chloroform) were used for infrared spectroscopy (IR, KBr), thermal analyses (DSC, TG) and for X-ray powder diffraction, see discussion below.

Both products **Fc-eda-boc** (**1**) and **Fc-eda-imda** (**2**) were characterized by $^1$H and $^{13}$C NMR, IR and UV-Vis spectroscopy and ESI mass spectrometry. The ESI MS spectra reveal molecular ions for both compounds, M+$Na^+$ and 2M+$Na^+$ for **1** and M+$H^+$ for **2**, at m/z 395.0, 767.1 and 539.1, respectively. In the UV-Vis ($CHCl_3$) spectra the characteristic ferrocene absorption peak is found at 443 nm for both **1** and **2**, suggesting that the substitution at the distant amide group moiety has no effect on the ferrocene chromophor.[19,20] Most interesting for the study of supramolecular interactions are the IR and NMR spectra. Secondary amide N-H groups without hydrogen bonding are characterized by stretching bands in the range 3500–3400 $cm^{-1}$, while hydrogen bonded secondary amide groups show these bands under 3400 $cm^{-1}$.[21] The IR (KBr) spectra are very similar for both samples $\mathbf{2}_{\mathbf{MeOH}}$ and $\mathbf{2}_{\mathbf{CHCl3}}$, showing NH stretching at 3276 and 3132 $cm^{-1}$, while the IR ($CHCl_3$) spectrum of **2** shows a band at 3284 $cm^{-1}$. In the $^1$H

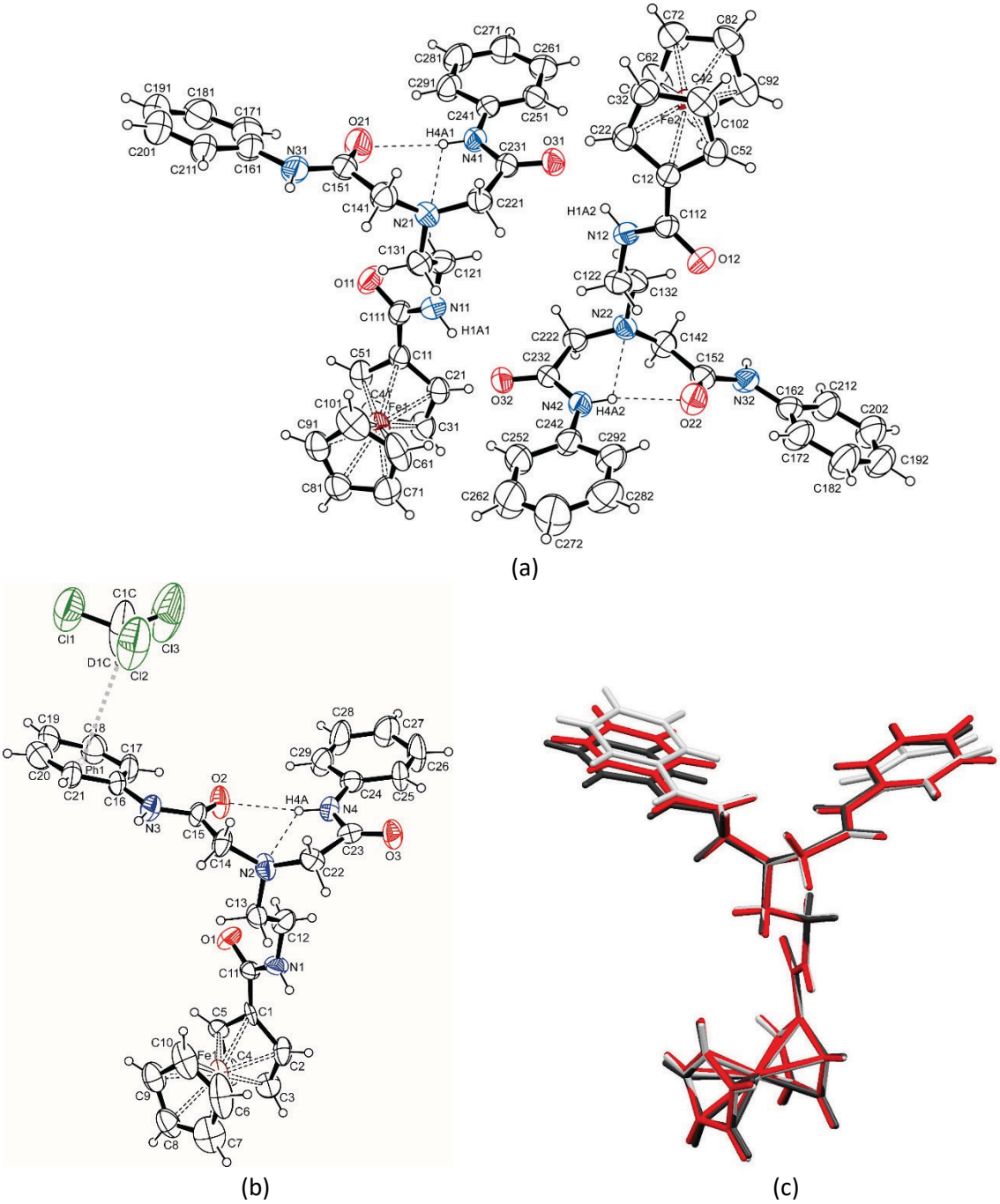


**Figure 1.** ORTEP-3 drawings[22] of molecular structures of compounds **2a** (a) and **2b** (b), with atomic numbering scheme. Intramolecular hydrogen bonds are shown as black dashed lines. C-H···π interaction in **2b**) is shown as grey dashed line (c) Overlap of three independent molecules of **2a** and **2b**, showing almost identical molecular conformation.

NMR ($CDCl_3$) spectrum of the title compound **2**, the amide proton peaks are found at 6.76 ppm (NH-eda) and 9.20 ppm (NH-imda). From the data we conclude that the amide groups are H-bonded in $CHCl_3$ solution of **2** as well as in solid state of both $\mathbf{2}_{\mathbf{MeOH}}$ and $\mathbf{2}_{\mathbf{CHCl3}}$.

## X-ray Single Crystal Structures

Molecular structures of **2a** and **2b**, with atomic numbering schemes are given in Figure 1;[22] the structural determination procedures are given in the Experimental part. In the crystal structure of **2a**, the asymmetric unit is

**Table 2.** Characteristic structural parameters for the ferrocene moiety in **2a** and **2b**.[21]

| moiety[a] | $\omega$[b] / ° | $\Theta$ / ° | $\beta$ / ° |
|---|---|---|---|
| **2a** | | | |
| Cp11···Fe1···Cp21 | 7.1(3)-7.8(3) | 2.5(4) | 20.8(7) |
| Cp12···Fe2···Cp22 | −2.0(7)-(−4.0(7)) | 2.4(4) | 19.1(5) |
| **2b** | | | |
| Cp1···Fe1···Cp2 | 3.4(8)–5.3(8) | 1.3(12) | 19.1(17) |

[a] Cp11 = C11, C21, C31, C41, C51; Cp21 = C61, C71, C81, C91, C101
Cp12 = C12, C22, C32, C42, C52: Cp22 = C62, C72, C82, C92, C102
Cp1 = C1, C2, C3, C4, C5; Cp2 = C6, C7, C8, C9, C10
[b] The range of C-Cg-Cg-C torsion angles, where C's are opposite carbon Cp atoms of ferrocene moiety and Cg are rings centroids.

formed by two **Fc-eda-imda** molecules related by a non-crystallographic center of symmetry. The crystal structure of **2b** consists of one **Fc-eda-imda** molecule and one chloroform solvent molecule. Important structural parameters of ferrocene amides reveal typical values; they include the torsion angle $\omega$ between the two cyclopentadienyl (Cp) rings, the tilt angle $\theta$ between the two Cp rings and the twist angle $\beta$ between the Cp ring and the amide plane (Table 2).[21] Angles at **imda** amine nitrogen atom (N21 and N22 in **2a** and N2 in **2b**) are typical for $sp^3$ hybridization. Molecular conformation of the three independent **Fc-eda-imda** molecules in **2a** and **2b** is almost identical, Figure 1c.

Figure 1 also shows the intramolecular hydrogen bonds listed in Table 3; in both structures **2a** and **2b** they exist between nitrogen atom N4 (N41 and N42 in **2a**) and oxygen atom O2 (O21 and O22 in **2a**). As the lone electron pair in the $sp^3$ hybridized atom N2 (N21 and N22 in **2a**) can act as the hydrogen bonding acceptor, intramolecular hydrogen bonds N4−H4A···N2 (N41−H41A···N21 and N42−H42···N22 in **2a**) should be considered as additional intramolecular stabilization interaction. In the literature, several examples of similar intramolecular hydrogen bonding in **imda** derivatives are described.[23,24]

In the single crystal structure of **2a**, two molecules in the asymmetric unit are connected with two N−H···O type of hydrogen bonds (N11−H1A1···O32 and N12−H1A2···O31, Figure 2a and Table 3), forming a pseudo-centrosymmetric ring pattern with graph-set notation $\mathbf{R_2^2(16)}$.[25] The same structural motif exists in the crystal structure of **2b**. Hydrogen bond N1−H1A···O3$^{v}$ (Table 3), together with its centrosymmetric equivalent, connects two molecules related by center of symmetry into a structural dimer having the same ring $\mathbf{R_2^2(16)}$ notation (Figure 2b).

Both crystallographic structures **2a** and **2b** show completely analogous 2D supramolecular aggregation as a consequence of other intermolecular N−H···O types of hydrogen bonds. In particular, in the structure of **2a**, hydrogen bond N31−H3A1···O12$^{i}$ (Table 3) forms a one-dimensional chain consistent with a two-fold screw symmetry axis extruding along the crystallographic axis *b* (Figure 2a). Second hydrogen bond N32−H3A2···O11$^{ii}$

**Table 3.** Hydrogen bonding parameters in **2a** and **2b** (including C-H···π interactions)

| | Distance/Å | | | Angle/° | Symmetry code |
|---|---|---|---|---|---|
| D-H···A[a] | D-H | H···A | D···A | D-H···A | |
| **2a** | | | | | |
| N11-H1A1···O32 | 0.86 | 2.10 | 2.923(6) | 159 | |
| N31-H3A1···O12$^{i}$ | 0.86 | 2.03 | 2.789(7) | 147 | $-x, -1/2+y, 1/2-z$ |
| N41-H4A1···O21 | 0.86 | 2.23 | 3.085(7) | 173 | |
| N41-H4A1···N21 | 0.86 | 2.30 | 2.736(6) | 111 | |
| N12-H1A2···O31 | 0.86 | 2.10 | 2.920(6) | 159 | |
| N32-H3A2···O11$^{ii}$ | 0.86 | 2.00 | 2.775(6) | 149 | $1-x, 1/2+y, 1/2-z$ |
| N42-H4A2···O22 | 0.86 | 2.16 | 3.016(6) | 170 | |
| N42-H4A2···N22 | 0.86 | 2.28 | 2.724(6) | 112 | |
| C31-H31···Ph4$^{iii}$ | 0.93 | 2.86 | 3.598(7) | 137 | $1+x, y, z$ |
| C32-H32···Ph2$^{iv}$ | 0.93 | 2.99 | 3.704(6) | 135 | $-1+x, y, z$ |
| **2b** | | | | | |
| N1-H1A···O3$^{v}$ | 0.86 | 2.10 | 2.93(2) | 161 | $1-x, -y, 1-z$ |
| N3-H3A···O1$^{vi}$ | 0.86 | 2.03 | 2.81(2) | 150 | $x, 1/2-y, -1/2+z$ |
| N4-H4A···O2 | 0.86 | 2.24 | 3.09(2) | 170 | |
| N4-H4A···N2 | 0.86 | 2.26 | 2.72(2) | 114 | |
| C1C-D1C···Ph1 | 0.98 | 2.98 | 3.89(4) | 155 | |

[a] For **2a**: Ph2 = C241, C251, C261, C271, C281, C291; Ph4 = C242, C252, C262, C272, C282, C292
For **2b**: Ph1 = C16, C17, C18, C19, C20, C21

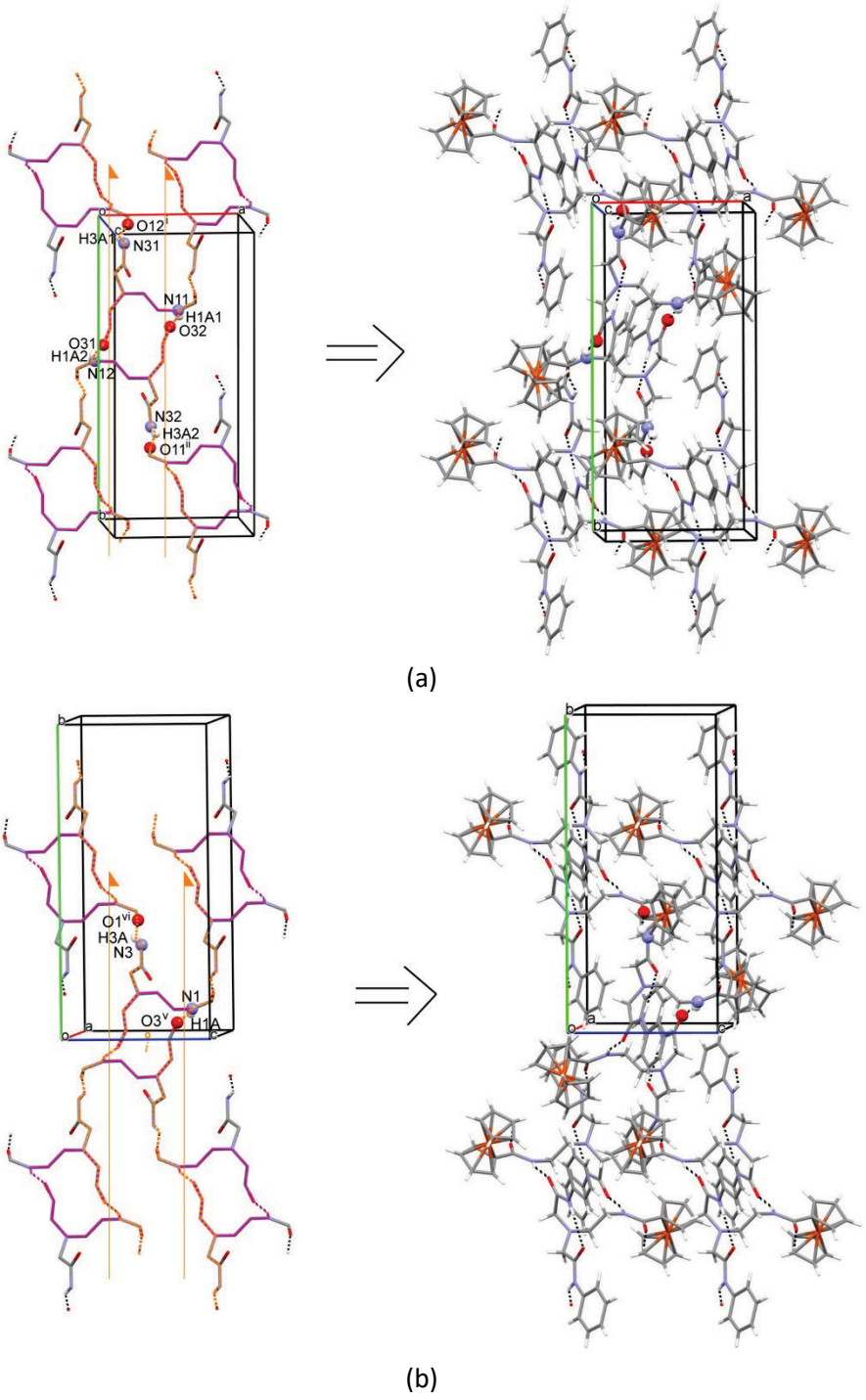


**Figure 2.** Intermolecular hydrogen bonding aggregation of molecules into 2D layers in **2a** (a) and **2b** (b). Atoms involved in hydrogen bonds are labelled and represented as small ball, other parts are represented in stick style. The left parts of pictures represent hydrogen bonding skeletons. Dimers formed by hydrogen bonds N11-H1A1···O32 and N12_H1A2···O31 in **2a** (a) and N1-H1A···O3$^{vi}$ in **2b** (b) are colored in purple and one-dimensional chains formed by other intermolecular hydrogen bonds (consistent with two-fold screw axes) are given in orange. One hydrogen bonded dimer (purple) is surrounded with four nearest neighbors, and layers formed by whole molecules are given in right part of pictures.

**Table 4.** Geometry parameters of selected interlayer π···π interactions in **2a** and **2b**

| Interaction[a] | Distance/Å Ph(i)···Ph(j) | Ph(i)-Perp[b] | Ph(i)-Perp[c] | Angle/° < Ph(i), Ph(j) | Symmetry code |
|---|---|---|---|---|---|
| **2a** | | | | | |
| Ph1···Ph1$^{vii}$ | 5.771(6) | 5.672(4) | 5.672(4) | 0 | $-x, -y, -z$ |
| Ph1···Ph4$^{viii}$ | 5.115(5) | 2.981(4) | 2.728(4) | 9.6(5) | $x, 1/2-y, -1/2+z$ |
| Ph2···Ph2$^{ix}$ | 4.885(4) | 3.238(3) | 3.237(3) | 0 | $-x, 1-y, -z$ |
| Ph3···Ph4$^{x}$ | 5.094(6) | 3.819(4) | 5.017(4) | 33.1(5) | $1-x, 1-y, 1-z$ |
| **2b** | | | | | |
| Ph2···Ph2$^{xi}$ | 5.719(12) | 3.957(9) | 3.958(9) | 0 | $-x, -y, 1-z$ |

[a] For **2a**: Ph1 = C161, C171, C181, C191, C201, C211; Ph2 = C241, C251, C261, C271, C281, C291; Ph3 = C162, C172, C182, C192, C202, C212; Ph4 = C242, C252, C262, C272, C282, C292
For **2b**: Ph2 = C24, C25, C26, C27, C28, C29.
[b] Perpendicular distance of Ph(i) on plane of Ph(j)
[c] Perpendicular distance of Ph(j) on plane of Ph(i)

(Table 3) also forms a one-dimensional chain extruding in the direction of axis *b*, but consistent with a two-fold screw axis which is not equivalent to the previous one: the second axis is moved in the direction of axis *a* by half of the period (Figure 2a). Therefore, a dimer of **Fc-eda-imda** molecules in the asymmetric unit **2a** is surrounded by four nearest neighboring equivalent dimers and 2D supramolecular aggregation in the *ab* plane of the unit cell is formed. In the structure of **2b**, the pseudo-centrosymmetric dimer is replaced by the exact structural dimer formed by the above mentioned hydrogen bond N1−H1A···O3$^{v}$. The role of the intermolecular hydrogen bond N3−H3A···O1$^{vi}$ (Table 3) is equivalent to the role of hydrogen bond N31−H3A1···O11$^{i}$ in the structure of **2a**, i.e. it forms a one-dimensional chain consistent with a two-fold screw axis extruding in the direction of axis *b* (Figure 2b). By combination of screw axis with the crystallographic center of symmetry existing in the center of the dimer in **2b**, a second screw axis is generated. This axis is moved in the direction of axis *c* by half of the period (Figure 2b). Again, the centrosymmetric dimers in **2b** are connected by four nearest neighbors in complete analogy with the structure of **2a**. In the case of **2b**, the 2D supramolecular aggregation is formed in the *bc* plane of the unit cell. In **2a**, this 2D supramolecular layer is additionally stabilized with two C−H···π interactions (C31−H31···Ph4$^{iii}$ and C32−H32···Ph2$^{iv}$ Table 3). In **2b** analogous interaction C3−H3···Ph2 is weaker because H3···Ph2 distance is larger than 3 Å.

It is interesting that similar, but not equivalent hydrogen bonding motifs are described in the literature for the crystal structure of nitrilotriacetanilide.[24] Intramolecular hydrogen bonds in that compound are completely analogous to those in **2a** and **2b**, while one type of intermolecular N−H···O hydrogen bonds form the centrosymmetric dimer that can also be described by the **$R_2^2$(16)** graph set notation.[25] However, the ring motif in nitrilotriacetanilide is not completely analogous to the ring motif in **2a** and **2b**, because it doesn't possess the -$CH_2$−$CH_2$- group and one amide group in the ring is reversely oriented compared with the one connected to the ferrocene in **2a** and **2b**. Finally, the other type of intermolecular N−H···O hydrogen bonds form additional connections of the centrosymmetric dimers in 1D ladder type of supramolecular aggregation, contrary to 2D layers encountered in **2a** and **2b**.

In the third spatial dimension, the supramolecular hydrogen bonded 2D layers in **2a** and **2b** are connected by weak van der Waals interactions or by weak π···π stacking interactions. Stacking interactions seem to be more important in **2a**. Several selected interactions are illustrated in Figure 3 and their geometry parameters are given in Table 4. Although the distances between centers of phenyl rings which are involved are significant (≈5 Å), the perpendicular distances of some ring centroids on the planes of associate rings are less than 3.4 Å, the value that can be used as the contact distance between two carbon atoms.[26] Also, it was recently demonstrated that stacking interactions exist even at larger distances.[27] As evident from Figure 3a, the neighboring 2D layers in the crystal structure of **2a** are not just translated in the stacking direction, but they are also shifted in direction of axis *b*. The stacking of neighboring layers in crystal structure of **2b** is different, the supramolecular hydrogen bonding 2D layers are now just translated in the stacking direction one above the other and a thin layer of chloroform molecules divides the layers (Figure 3b). Chloroform solvent molecules interact with the 2D layers only by one C−D···π interaction (C-D group from chloroform and Ph1 phenyl ring from the **Fc-eda-imda** molecule (Figure 1b and Table 3) and by weak Van der Waals interactions with surrounding molecules. If we take into account weak long range π···π interactions, only one interaction could be recognized, Ph2···Ph2$^{xi}$ (Table 4).

In the crystal packing of molecules, different stacking of analogous 2D hydrogen bonded layers is often a source of polymorphism.[28–30] From presented analysis it is

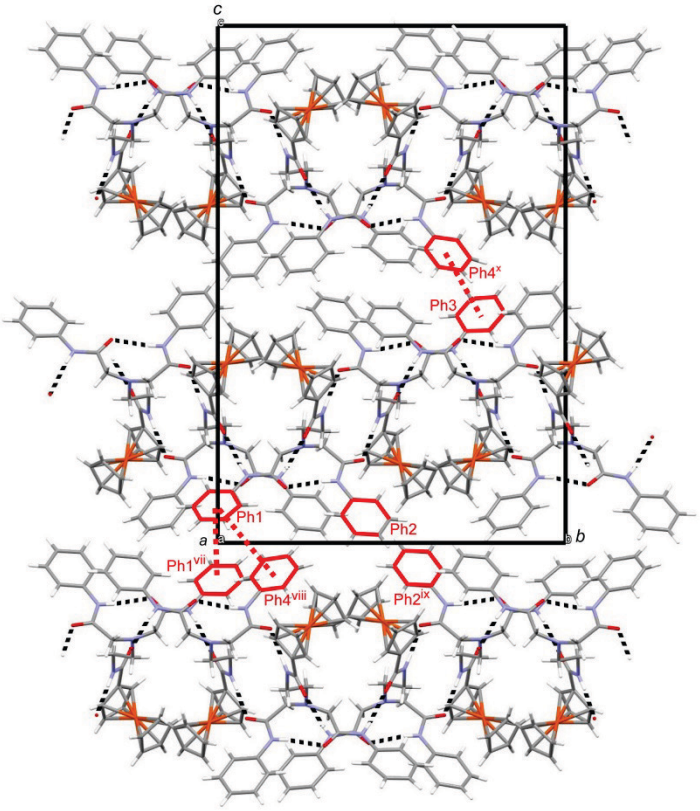


(a)

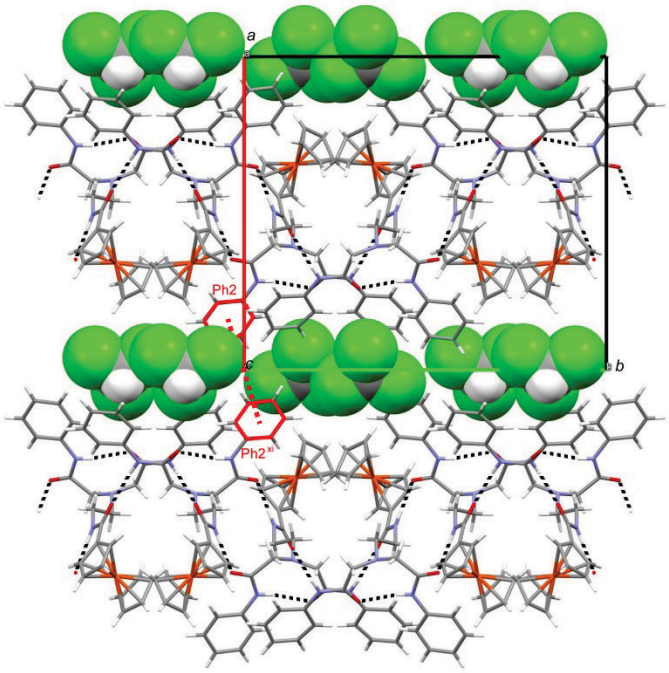


(b)

**Figure 3.** Representation of stacking of hydrogen bonded layers in third dimension in **2a** (a) and **2b** (b), where selected π···π interactions are labelled and colored in red. In case of crystal packing in **2b**, layers formed by solvent chloroform molecules are represented in space-filling (CPK) style.

evident that the difference in crystal packing in structures of **2a** and **2b** comes from additional chloroform (solvent) molecules present only in crystal structure of **2b**. Solvent molecules in the crystal structure can induce crystal packing in different crystal symmetries, however, in this work both crystal structures **2a** and **2b** are consistent with the $P2_1/c$ space group.

## Thermal Analysis and Powder Diffraction

In the DSC thermograms, the melting points of bulk powder samples $\mathbf{2}_{\mathbf{MeOH}}$ and $\mathbf{2}_{\mathbf{CHCl3}}$ are sharp peaks at approximately 210 °C for both samples and the decomposition of compounds is observed as wide peaks at approximately 270 °C for both compounds. Compound $\mathbf{2}_{\mathbf{CHCl3}}$ has an additional peak at 95 °C which corresponds to the loss of chloroform molecules from the crystal structure. This temperature is above the boiling point of chloroform due to chloroform molecules being trapped in the crystal structure.

The TG thermograms of $\mathbf{2}_{\mathbf{MeOH}}$ and $\mathbf{2}_{\mathbf{CHCl3}}$ support the DSC results; the thermograms of both samples are very similar in the later part, showing melting of the compounds with decomposition (120–450 °C). Also similar to DCS analysis, $\mathbf{2}_{\mathbf{CHCl3}}$ shows loss of chloroform. However, the chloroform loss is not in a stoichiometric amount, indicating that a mixture of **2a** and **2b** is present in the sample of $\mathbf{2}_{\mathbf{CHCl3}}$. In particular, instead of 18.15 % weight loss which would correspond to one chloroform molecule, the observed weight loss was 6.02 %, showing that the $\mathbf{2}_{\mathbf{CHCl3}}$ sample contains about 67 % of **2a** and 33% of **2b**.

The powder diffractogram of $\mathbf{2}_{\mathbf{MeOH}}$ is in agreement with the single crystal X-ray structure of **2a** (see Supplementary material), strongly supporting the conclusion that sample $\mathbf{2}_{\mathbf{MeOH}}$ contains only **2a**. The results obtained from $\mathbf{2}_{\mathbf{CHCl3}}$ suggest that it is a mixture in a ratio of approximately of 65% of **2a** and 35% of **2b**, in good agreement with TG results.

When comparing these results with the observed crystal habitus of bulk powder samples $\mathbf{2}_{\mathbf{MeOH}}$ and $\mathbf{2}_{\mathbf{CHCl3}}$: a single type of flower-like crystals was obtained in $\mathbf{2}_{\mathbf{MeOH}}$ indicating a pure sample of **2a**, while a mixture of flower-like **2a** and needle-like **2b** crystals was obtained in $\mathbf{2}_{\mathbf{CHCl3}}$.

**Acknowledgment.** Financial support of Croatian Science Foundation (IP-2014-09-1461) is gratefully acknowledged. The research visit of undergraduate student Jeremy Le Pennec (Ensi CAEN, France) at the Ruđer Bošković Institute was supported by an ERASMUS scholarship. The authors thank Ernest Sanders (RBI) for technical assistance, dr. sc. Neven Smrečki (Faculty of Science, University of Zagreb) for recording the DSC thermograms, dr. sc. Igor Milanović (RBI) for recording the powder diffractograms and dr. sc. Zoran Štefanić (RBI) for recording the single crystal diffraction.

**Supplementary Information.** Supporting information to the paper is attached to the electronic version of the article at: http://doi.org/10.5562/cca3270. It contains NMR, IR, UV-Vis and mass spectra, DSC and TG thermograms and X-ray powder diffractograms.

## REFERENCES

[1] (a) C. J. Pedersen, *J. Am. Chem. Soc.* **1967**, *89*, 2495; (b) J.-M. Lehn, *Supramolecular Chemistry: Concepts and Perspectives*, Wiley-VCH, Weinheim, Germany, **1995**.

[2] I. V. Kolesnichenko, E. V. Anslyn, *Chem. Soc. Rev.* **2017**, *46*, 2385.

[3] J. Li, D. Yim, W.-D. Jang, J. Yoon, *Chem. Soc. Rev.* **2017**, *46*, 2437.

[4] S. Kassem, T. van Leeuwen, A. S. Lubbe, M. R. Wilson, B. L. Feringa, D. A. Leigh, *Chem. Soc. Rev.* **2017**, *46*, 2592.

[5] M. J. Webber, R. Langer, *Chem. Soc. Rev.* **2017**, *46*, 6600.

[6] P. W. N. M. van Leeuwen (Ed.), *Supramolecular Catalysis*, Wiley-VCH, Weinheim, Germany, **2008**.

[7] S. Hecht, I. Huc (Eds.), *Foldamers*, Wiley-VCH, Weinheim, Germany, **2007**.

[8] (a) N. Smrečki, O. Jović, B.-M. Kukovec, E. Šimunić, S. Vuk, A. Skuhala, M. Babić, T. Rončević, N. Ilić, I. Kekez, D. Matković-Čalogović, Z. Popović, *Inorg. Chim. Acta* **2018**, *471*, 521; (b) N. Smrečki, B.-M. Kukovec, M. Đaković, Z. Popović, *Polyhedron* **2015**, *93*, 106; (c) M. Sekizaki, *Bull. Chem. Soc. Jpn.* **1974**, *47*, 1447.

[9] For closely related bis(2-picolyl)amine (**bpa**) ligands see for example: (a) Đ. Škalamera, E. Sanders, R. Vianello, A. Maršavelski, A. Pevec, I. Turel, S. I. Kirin, *Dalton Trans.* **2016**, *45*, 2845; (b) S. I. Kirin, I. Ott, R. Gust, W. Mier, T. Weyhermüller, N. Metzler-Nolte, *Angew. Chem. Int. Ed.* **2008**, *47*, 955.

[10] (a) T. Moriuchi, T. Hirao, *Acc. Chem. Res.* **2010**, *43*, 1040; (b) D. R. van Staveren, N. Metzler-Nolte, *Chem. Rev.* **2004**, *104*, 5931; (c) M. Čakić Semenčić, L. Barišić, Croat. Chem. Acta, 90 (2017) in press, doi:10.5562/cca3246.

[11] A. C. Larson, R. B. Von Dreele, *"General Structure Analysis System (GSAS)", Los Alamos National Laboratory Report LAUR*, **1994**, 86.

[12] B. H. Toby, *J. Appl. Cryst.* **2001**, *34*, 210.

[13] CrysAlisPro, Rigaku OD, Version 1.171.38.43, **2015**.

[14] M. C. Burla, R. Caliandro, M. Camalli, B. Carrozzini, G. L. Cascarano, C. Giacovazzo, M. Mallamo, A. Mazzone, G. Polidori, R. Spagna, *J. Appl. Cryst.* **2012**, *45*, 357.

[15] F. L. Hirshfeld, *Acta Cryst.* **1976**, *A32*, 239.

[16] G. M. Sheldrick, *Acta Cryst.* **2008**, *A64*, 112.
[17] E. Müller, O. Bayer, H. Meerwein, K. Ziegler, *Methoden der Organischen Chemie* (*Houben Weyl*), *Band XI/2 – Stickstoffverbindungen II und III*, Georg Thieme Verlag, Stuttgart **1958**.
[18] S. Martić, M. Labib, D. Freeman, H.-B. Kraatz, *Chem. Eur. J.* **2011**, *17*, 6744.
[19] For a similar building block, **Fc-CO-NH-$CH_2$-$CH_2$-NH-$CH_2$-$CO_2$-*t*Bu**, see: L. A. Levine, S. I. Kirin, C. P. Myers, S. A. Showalter, M. E. Williams, *Eur. J. Inorg. Chem.* **2009**, 613.
[20] S. I. Kirin, D. Wissenbach, N. Metzler-Nolte, *New J. Chem*. **2005**, 29, 1168.
[21] S. I. Kirin, H.-B. Kraatz, N. Metzler-Nolte, *Chem. Soc. Rev.* **2006**, *35*, 348.
[22] L. J. Farrugia, *J. Appl. Cryst.* **2012**, *45*, 849.
[23] L. Rajput, P. Sanphui, K. Biradha, *Cryst. Growth Des.* **2007**, 7, 1872.
[24] J. M. Rowland, G. J. Ibanez, M. M. Olmstead, M. Ruf, P. K. Mascharak, *Acta Crystallogr., Sect. E: Struct. Rep. Online* **2001**, *57*, o1001.
[25] J. Bernstein, R. E. Davis, L. Shimoni, H.-L. Chang, *Angew. Chem. Int. Ed.* **1995**, *34*, 1555.
[26] A. Spek, *J. Appl. Cryst.* **2003**, *36*, 7.
[27] R. Kruszynski, T. Sierański, *Cryst. Growth Des*. **2016**, *16*, 587.
[28] K. Užarević, Z. Kokan, B. Perić, N. Bregović, S. I. Kirin, *J. Mol. Struct.*, **2013**, *1031*, 160.
[29] H. G. Brittain, *Polymorphism in Pharmaceutical Solids*, 2nd Edition, CRC Press, **2009**, p. 233.
[30] M. Jurić, B. Perić, N. Brničević, P. Planinić, D. Pajić, K. Zadro, G. Giester, B. Kaitner, *Dalton Trans.* **2008**, 742.